Journal of Rock Mechanics and Geotechnical Engineering 18 (2026) 4034–4049

Contents lists available at ScienceDirect

Journal of Rock Mechanics and Geotechnical Engineering

journal homepage: www.jrmge.cn

Full Length Article

Efficient stabilization of dredged sediment by combining nano-modification and low-carbon supersulfated cement

Lei Lang [a,*], Dongxing Wang [b], Bing Chen [c], Desheng Li [d], Linlin Gu [d,**]

[a] School of Architecture and Planning, Yunnan University, Kunming, 650500, China
[b] School of Civil Engineering, Wuhan University, Wuhan, 430072, China
[c] State Key Laboratory of Ocean Engineering, Shanghai Jiao Tong University, Shanghai, 200240, China
[d] School of Safety Science and Engineering, Nanjing University of Science and Technology, Nanjing, 210094, China

ARTICLE INFO

Article history:
Received 22 January 2025
Received in revised form
10 June 2025
Accepted 18 August 2025
Available online 10 October 2025

Keywords:
Nano-modification
Supersulfated cement
Dredged sediment stabilization
Strength development
Micro-mechanism

ABSTRACT

Supersulfated cement (SSC) is considered an environmentally friendly alternative to ordinary Portland cement (OPC), while its stabilization efficiency on dredged sediment (DS) is still unclear. Three types of SSC were prepared by combining ground granulated blast-furnace slag, alkali-activator NaOH, and a sulfate waste source, yielding SSCE (from electrolytic manganese residue), SSCP (from phosphogypsum), and SSCD (from desulfurization gypsum). To further enhance the stabilization efficiency of SSC on DS, nano-SiO_2 (NS) and nano-Al_2O_3 (NA) were incorporated individually and as a composite blend. Mechanical properties and microstructural analyses were conducted to evaluate the stabilization efficiency and elucidate the underlying mechanisms. The leaching toxicity of SSCE-stabilized DS was investigated via leaching tests. The results showed that both alkali-activation and nano-modification can significantly improve the strength development of SSC-stabilized DS. At least 15 % NaOH was required for SSC to achieve the same stabilization efficiency as OPC. The optimum NA-modified SSCD-stabilized DS demonstrated superior strength compared to OPC-stabilized DS. Composite NS/NA-modification was more efficient than using NS or NA individually. For DS stabilized with SSCE, SSCP, and SSCD, the optimal NS-to-NA mass ratios were 7:3, 3:7, and 3:7, respectively. Notably, the nano-modified SSCE-stabilized DS showed no environmental risks. Incorporating NS and NA into SSC-stabilized DS respectively promoted the formation of C-S-H gel and ettringite. A micro-mechanism model was developed to explain the strength evolution of nano-modified SSC-stabilized DS. This study provides a theoretical basis for the application of SSC in DS stabilization, and facilitates the collaborative resource utilization of industrial solid wastes and DS.

1. Introduction

The rapid advancement of urbanization and port construction in coastal areas has led to a sharp increase in dredged sediment (DS) generation, driven by more frequent dredging projects for navigation channels, water environmental treatment, and marine waterways (Liu et al., 2023; Wang et al., 2024a). Unlike common soft soils, DS has typical engineering defects such as high water content, low strength, rich in fine-grained clay particles and organic matter, seriously restricting its resource utilization (Wang et al., 2023; Lang et al., 2024a). Specifically, high water content is the most typical characteristic that distinguishes DS from soft soil. Usually, DS has water content exceeding the liquid limit, thus exhibiting the flowing or flow-plastic state. Consequently, fresh DS requires time-consuming pre-treatment in sedimentation tanks before being transported to a suburban storage yards (Xu et al., 2023). These processes entail significant environmental burdens, high transportation costs, and extensive land occupation. Therefore, recycling DS as a renewable construction material is mandatory to mitigate these environmental and economic challenges.

Stabilization is an effective technology for strengthening and utilizing DS, and cement-based binders are widely used for this

* Corresponding author.
** Corresponding author.
E-mail addresses: langleijy@126.com (L. Lang), linlin_gu@njust.edu.cn (L. Gu).

Peer review under responsibility of Institute of Rock and Soil Mechanics, Chinese Academy of Sciences.

https://doi.org/10.1016/j.jrmge.2025.08.013

purpose due to their cost-effectiveness, wide applicability, and abundant supply (Lang et al., 2024b; Zhang et al., 2025). However, the inherently high water content of DS necessitates large cement dosages to achieve the required design strength requirement, thereby reducing stabilization efficiency (Li et al., 2022). Furthermore, the cement production and application are associated with CO_2 emission, high consumption of energy and non-renewable resources (Hossain et al., 2020; Li and Yi, 2023). Therefore, developing an alternative binder that is high efficiency, low-carbon, economic, and wide applicable for stabilizing high water content DS is crucial for advancing green and sustainable development.

Supersulfated cement (SSC) is a sustainable cementitious material primarily composed of ground granulated blast-furnace slag (GGBS) and sulfate (Wang et al., 2024b). The sulfate component can be derived from sulfate solid wastes like electrolytic manganese residue (EMR), phosphogypsum (PG), and desulfurization gypsum (DG) (Tang et al., 2024). Therefore, SSC is an ideal sustainable alternative to OPC due to its low-carbon, low energy consumption, and cheap raw material prices (Wu et al., 2021). GGBS is an industrial solid waste and exhibits more environmentally friendly and cost-effective properties than OPC (Chen et al., 2024a). However, the hydration rate of GGBS is low, and alkali-activation is commonly adopted to accelerate the potential activity of GGBS (Zhang et al., 2023). Sodium hydroxide (NaOH) is widely used as an alkali activator of GGBS, facilitating the breakage of Si-O, Ca-O, and other stable structures inside GGBS, and thus promoting the hydration process (Li et al., 2023). However, the use of alkali-activator NaOH also introduces CO_2 emission, energy consumption, and high cost (Lang et al., 2025). EMR is generated during the leaching and ammonia neutralization process of manganese carbonate ore, and its major chemical compositions are SiO_2, Al_2O_3, and $CaSO_4{\cdot}2\ H_2O$ (Wu et al., 2024). PG is a residue product of wet-process phosphoric acid, mainly composed of calcium sulfate dihydrate, a small amount of phosphoric acid, fluoride, and other substances (Ren et al., 2023). DG is a by-product generated during wet flue gas desulfurization, mainly composed of calcium sulfate dehydrate (Xu et al., 2017). These three sulfate solid wastes can supply additional SO_4^{2-} for alkali-activated GGBS cementitious system and contribute to the production of ettringite (AFt). The generation of AFt not only improves the strength gain of the cemented matrix, but also combines with a large amount of free water (Chen et al., 2024b). These two aspects are essential for stabilizing DS with high water content. However, current research on SSC mainly focuses on its low-carbon modification, performance evaluation, and application in concrete (Wu et al., 2021; Sun et al., 2022; Xing et al., 2023; Tang et al., 2024; Wang et al., 2024b; Cao et al., 2024; Xu et al., 2024; Chang et al., 2024; Kang et al., 2024), and the stabilization feasibility and efficient of SSC on DS with high water content are still limited, as well as the corresponding micro-mechanism is also unknown. Furthermore, SSC has a typical problem of low early strength, which may be more severe when stabilizing DS with high water content, thereby weakening its stabilization efficiency.

In recent years, nanomaterials have been widely used in cementitious materials modification and soft soil stabilization (Zhang et al., 2021; Tsardaka et al., 2022; Aksu and Eskisar, 2023; Chen et al., 2024c). This is because nanomaterials have high purity, ultra-fine particle size, high pozzolanic reactivity, and specific surface area (Dai et al., 2024). For common nanoparticles, Nano-SiO_2 (NS) has gained significant attention for its excellent performance (Li et al., 2025). Beyond its nano-filling and nucleation induction effects, NS can directly react with calcium hydroxide to form cementitious gels, enhancing the hydration cementation ability of cement-based materials (Liu et al., 2022). Similar observations were also observed by Liu et al. (2021) and Shi et al. (2020), who found that adding NS can improve the mechanical and hydration properties of cement-slag cementitious systems. Furthermore, nano-$CaCO_3$, nano-MgO, and nano-ZnO have also been confirmed to be effective for increasing soft soil stabilization efficiency (Choobbasti et al., 2019; Yao et al., 2019; Khodaparaast et al., 2021). It can be deduced that the nano-modification actions promote the cement hydration and produce more cementitious gels, thus improving the hydration-bonding performance of cement-based materials. Wang et al. (2024b) found that incorporating nano-ettringite can enhance the compressive strength of SSC-based foamed concrete and promote the generation of hydration products, especially AFt. Similarly, Wang et al. (2024c) found that adding nano-Al2O3 (NA) can promote the production of AFt inside calcium sulphoaluminate cement and associated bonding strength improvement. Therefore, using suitable nanomaterials as an additive for SSC is expected to effectively improve its stabilization efficiency on DS. However, relevant studies are still deficient, and the corresponding micro-mechanisms are not yet clear.

This study aims to promote the synergistic utilization of industrial solid wastes and waste DS, thereby reducing environmental and economic burdens. The low-carbon SSC composed of alkali-activator NaOH, GGBS, and sulfate solid wastes (EMR, PG, and DG) was prepared for DS stabilization, and nanomaterials, including NS and NA, were incorporated as additives to enhance stabilization efficiency. The effects of alkali-activation and nano-modification on the stabilization efficiency were evaluated through strength evolution. Furthermore, the leaching toxicity, XRD, SEM, and TG-DTG tests were also performed to clarify the environmental risks and underlying strength-gain mechanisms. The key findings are expected to provide a theoretical basis and data support for the application of SSC in DS stabilization and advance the collaborative resource utilization of waste DS and industrial solid wastes.

2. Experimental program

2.1. Raw materials

The DS used in this study was collected from a dredging project in the Qingdao coastal area. The fresh DS has undergone a brief natural dehydration process, resulting in a decrease in water content, and it was dark grey in color and exhibited a fluid plastic state. Table 1 presents the physical performances of DS, which were tested as per GB/T 50123-2019 (2019). Fig. 1a and b shows the SEM image and XRD pattern of DS, indicating that the soil particles with flake and irregular shapes are loosely distributed, and the mineral compositions are mainly clay minerals. By conducting X-ray fluorescence (XRF) test, the chemical composition of DS was obtained and listed in Table 2, indicating that SiO_2 and Al_2O_3 are the main chemical compositions of DS.

Three types of low-carbon SSC (SSCE, SSCP, and SSCD) were prepared with alkali-activator NaOH, GGBS, and a sulfate source

Table 1
The basic physical properties of the used DS.

Property	Value
Initial water content (%)	57.3
Plastic limit (%)	23.1
Liquid limit (%)	37.8
Plasticity index (%)	14.7
Specific gravity	2.69
Optimum water content (%)	26.9
Maximum dry density (g/cm^3)	1.66

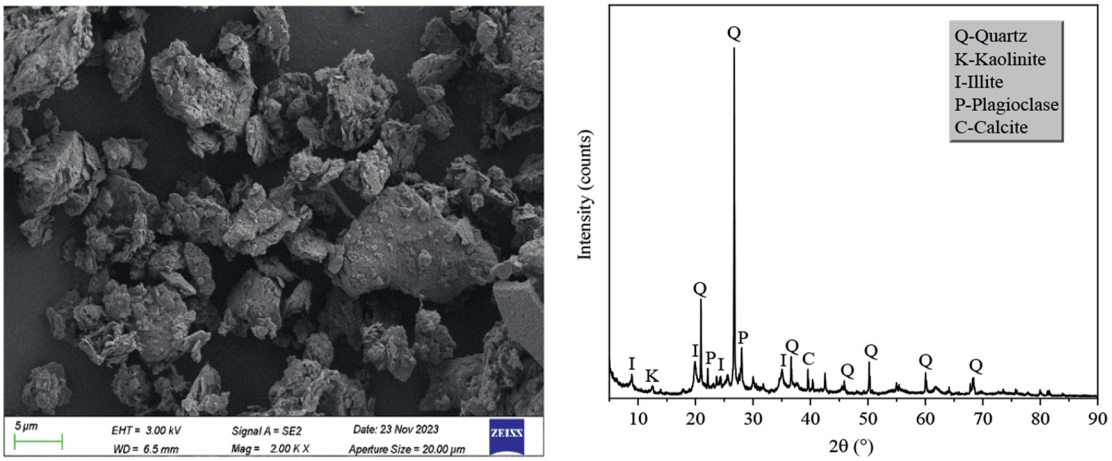

Fig. 1. The (a) microstructure and (b) crystalline phases of DS used in this study.

Table 2
Chemical compositions of raw materials.

Raw material	Chemical composition (%)								
	CaO	SiO_2	Al_2O_3	Fe_2O_3	MgO	K_2O	Na_2O	SO_3	Others
DS	0.8	51.89	18.93	6.72	2.64	2.98	2	–	14.04
GGBS	35.58	36.1	16.32	1.09	6.32	0.59	0.9	–	3.1
EMR	13.47	33.94	11.34	3.76	3.12	2.04	0.63	28.5	3.2
PG	33.2	8.55	1.38	0.56	0.23	0.38	0.11	53.85	1.74
DG	38.26	2.31	0.84	0.3	0.87	0.17	0.14	56.94	0.17

(EMR, PG, and DG), in which the mass ratio of GGBS to sulfate solid waste was fixed at 4:1, based on preliminary experiments and conventional SSC compositions. For example, the SSCE was prepared using NaOH, GGBS, and EMR under the GGBS-EMR mass ratio of 4:1, and the same synthesis method was also used for preparing SSCP and SSCD. Nano-SiO_2 (NS) and nano-Al_2O_3 (NA) were used as single and composite modifiers. The powdery S95 grade GGBS was provided by a manufacturer in Gongyi city, Henan Province, China. The EMR was collected from Guizhou Province, China. The pH and water content of fresh EMR are respectively 6.25 and 14.5 %. The used EMR was pre-treated by oven-drying, grinding and sieving (0.154 mm). The powdery PG and DG were purchased from a manufacturer located in Zhengzhou city, Henan Province, China. Analytical grade NaOH was used as the activator. The microstructure, crystalline phases, and chemical compositions of GGBS, EMR, PG, and DG are respectively shown in Figs. 2 and 3 and Table 2. The XRD pattern of GGBS in Fig. 3 shows no distinct crystalline peaks, indicating its amorphous structure and potential pozzolanic activity, while gypsum ($CaSO_4{\cdot}2\ H_2O$) was the main mineral inside EMR, PG, and DG. The SEM image of NS and NA is shown in Fig. 4, and their physical properties are given in Table 3.

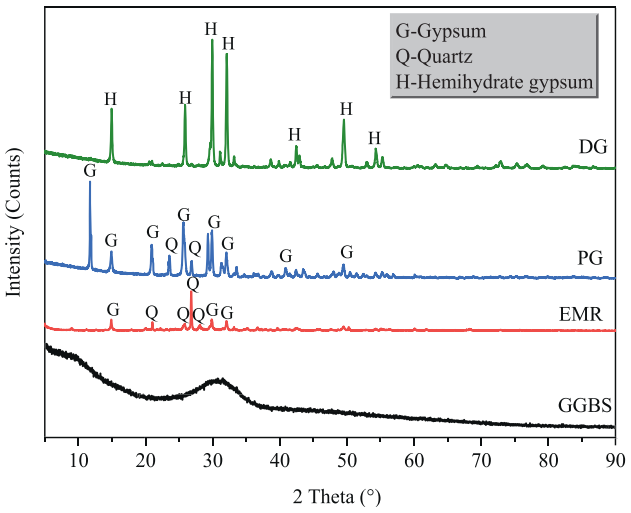

Fig. 2. The XRD patterns of raw materials, including GGBS, EMR, PG, and DG.

2.2. Sample preparation

The DS was first oven-dried at 60 °C, then milled and passed through a 2-mm sieve. To simulate the flow-state DS on site, the water content of experimental DS was adjusted to 90 % of the dry weight of DS, which is more than 1.5 times its initial water content. The dosage of GGBS-EMR/PG/DG binary binder was controlled at 20 % of the dry weight of DS. The NaOH content was designed to be 5 %, 10 %, 15 % and 20 % of the dry weight of the binary binder. Simultaneously, the 20 % ordinary Portland cement (OPC)-stabilized DS (CDS) was also used as a comparison to evaluate the stabilization efficiency of SSC on DS. The single NS and NA, as well as composite NS/NA, were used as the nano-modifiers of SSC. Based on the dry mass of SSC, the single nano-modifier content was 2 %–10 % with an interval of 2 %. Under a controlled dosage of 6 %, the mass ratio of NS to NA in composite nano-modifiers NS/NA was designed as 1/9, 3/7, 5/5, 7/3, and 9/1. The specific mix design of stabilized DS is shown in Table 4.

Based on Table 4, the deionized water and raw materials were weighed. The deionized water was then divided into three

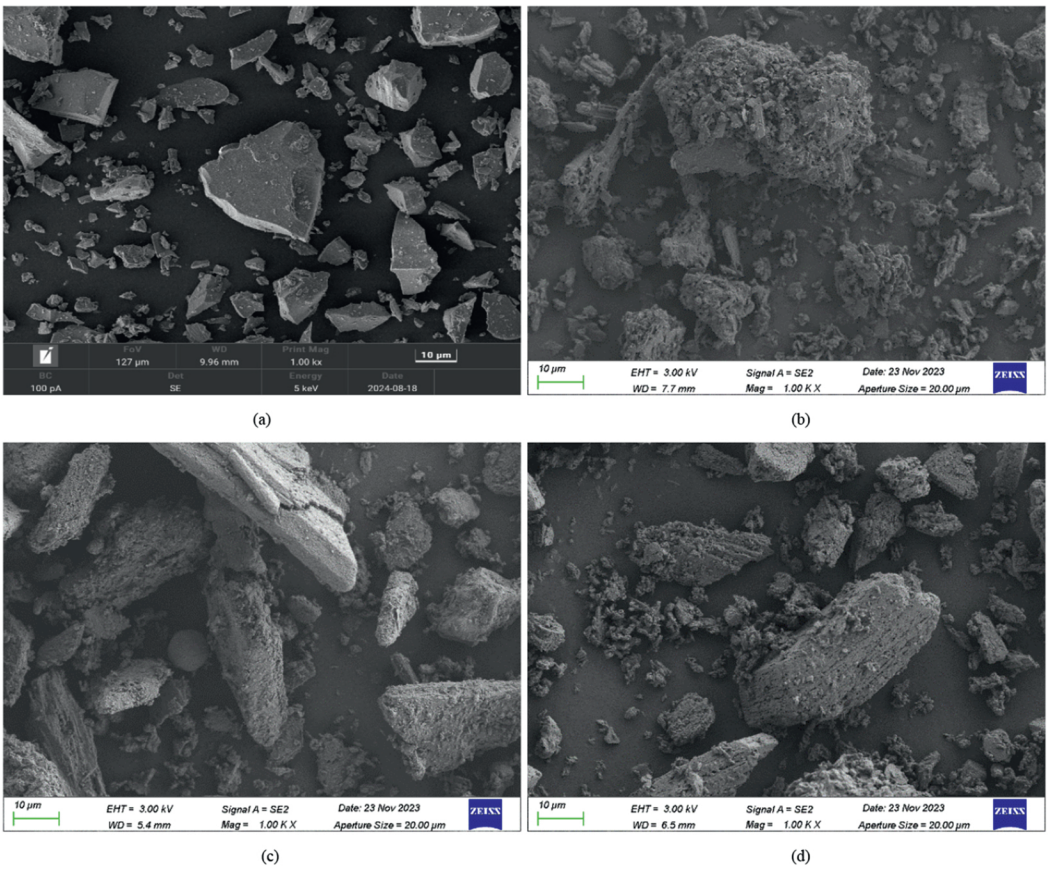

Fig. 3. The microstructure of (a) GGBS, (b) EMR, (c) PG, and (d) DG.

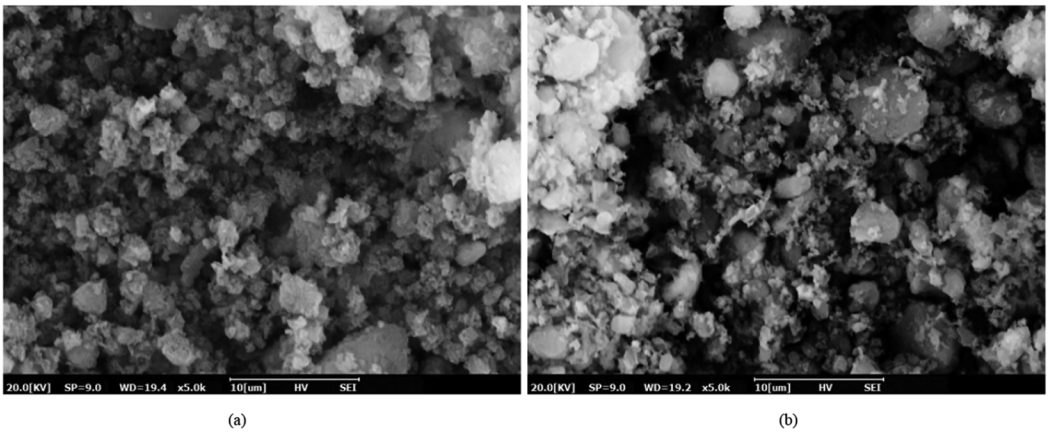

Fig. 4. The microstructure of (a) NS and (b) NA.

Table 3
Basic physical properties of NS and NA.

Nanomaterials	Purity (%)	APS (nm)	SSA (m^2/g)	Density (g/cm^3)	Phase
NS	99.8	15	230	0.13	NWP
NA	99.9	30	160	0.9	

Notes: APS is short for average particle size; SSA is short for specific surface area; and NWP is short for non-crystalline white powder.

portions: one for preparing the NaOH solution, a second for the stable nano-suspension, and the third of adjusting the water content of the mixture. The dry binary binder and DS were firstly mixed using an electric mixer to achieve a uniform dry mixture, then the prepared NaOH solution and nano-suspension were sequentially added and continued mixing for 5 min until the uniform nano-modified SSC-stabilized DS slurry was obtained. The well-prepared stabilized DS slurry was gradually poured into the PVC cylindrical molds (diameter × height = 50 mm × 50 mm), and vibration compacting was conducted to ensure uniform relative density. Three duplicate samples were prepared to ensure the validity of test results. The well-prepared samples together with molds were wrapped in vinyl bags, and demolding was conducted

Table 4
The mix design of SSC-stabilized DS.

Stabilized DS type	Binder type	NaOH content (%)	NS content (%)	NA content (%)	NS-NA mass ratio (6 %)
CDS	OPC	–	–	–	–
SEDS	SSCE	5, 10, 15, 20			
SPDS	SSCP				
SDDS	SSCD				
NS-modified SEDS, SPDS, and SDDS	NS-SSCE, NS-SSCP, NS-SSCD	10	2, 4, 6, 8, 10	–	–
NA-modified SEDS, SPDS, and SDDS	NA-SSCE, NA-SSCP, NA-SSCD		–	2, 4, 6, 8, 10	–
NS/NA-modified SEDS, SPDS, and SDDS	NS/NA-SSCE, NS/NA-SSCP, NS/NA-SSCD		0.6-5.4	0.6-5.4	1/9, 3/7, 5/5, 7/3, 9/1

Notes: SSCE is short for EMR-based SSC, SEDS is short for SSCE-stabilized DS, NS-SSCE is short for NS-modified SSCE, and others follow the same abbreviation rules.

after curing for 3 d. The stabilized samples after demolding were further cured under a standard curing box ((23 ± 2) °C and 95 % RH) until performing the subsequent strength and microstructural tests.

2.3. Testing methods

2.3.1. Unconfined compressive strength (UCS) test

A universal testing machine was used to determine the UCS of stabilized DS samples, as per ASTM D2166-16 (2016). During the testing, the compression load was applied at a constant rate of 1 mm/min until the sample failed, then the UCS of stabilized DS samples can be obtained. The average of three parallel results was the final result, and when the deviation was less than 5 %, the final result was confirmed to be valid. After UCS tests, the typical 28-d crushed samples were gathered for subsequent microstructural tests and analysis.

2.3.2. Leaching test

EMR contains heavy metals and pollutants such as manganese (Mn) and ammonia nitrogen (NH_4^+-N). The leaching toxicity of SSCE-stabilized DS was investigated, and the Chinese Standard HJ/T 299-2007 (2007) was adopted to measure the mass fraction of heavy metals and pollutants from leaching. Under the designed liquid-to-solid ratio of 10:1, the 10 g milled stabilized DS sample was mixed with 100 mL solution with a sulfuric acid-nitric acid mass ratio of 2:1 and a pH of 3.2 to prepare the leaching solution. Then, the leaching solution was oscillated at (110 ± 10) min^{-1} for (18 ± 2) h, and the leaching solution was filtered through a membrane with an aperture size of 45 μm. Lastly, the heavy metal leaching was determined by using an Agilent 7700 inductively coupled plasma optical emission spectrometer (ICP-OES). Furthermore, the concentration of ammonia nitrogen (NH_4^+-N) from leaching solution was tested via the Nessler's reagent spectrophotometric method. The leaching concentrations of various heavy metals and NH_4^+-N were compared with the Standard limits in GB 5085.3-2007 (2007) to evaluate the environmental risks.

2.3.3. X-ray diffraction (XRD)

The qualitative analysis of crystalline phases and mineral composition of typical 28-d stabilized DS samples was performed by XRD tests. The dried samples were ground into powder with a pestle in an agate mortar and sieved through a 200-mesh sieve, then the crystalline phases were scanned over a 2θ range of 10°–80° and at a scanning rate of 2°/min. The test results were further analyzed using MDI Jade 6 software.

2.3.4. Scanning electron microscopy (SEM)

The microstructural analysis of typical 28-d stabilized DS samples was conducted via scanning electron microscopy (SEM) tests. After UCS tests, some typical sample pieces were soaked in anhydrous alcohol to inhibit continuous hydration. Before SEM testing, the thin slice samples were prepared and coated with a layer of gold on the surface to ensure the clear microscopic morphology.

2.3.5. Thermogravimetric analysis (TG-DTG)

TG-DTG analysis was performed to identify the generation of various hydration products inside stabilized DS samples under different temperature ranges. The sample preparation for TG tests was identical to that for the XRD tests. Approximately 10 mg of the powdered sample was heated from 30 °C to 1000 °C at a heating rate of 10 °C/min under a nitrogen environment. Then, the TG curves together with DTG values were used to determine the weight loss associated with the decomposition of various products.

3. Results and analysis

3.1. Effect of alkali-activation

The effect of NaOH content on the strength evolution of three types of SSC (SSCE, SSCP, and SSCD) stabilized DS is shown in Fig. 5, and the corresponding strength of 20 % OPC-stabilized DS (CDS) is also listed as a control comparison. The UCS of SSCE-stabilized DS (SEDS) versus NaOH content is given in Fig. 5a, indicating that increasing NaOH content enhances the strength enhancement of SEDS. This confirms that incorporating NaOH accelerates the hydration process of SSCE and improves its stabilization efficiency for DS. It should be explained that the 7-d SEDS containing 5 % and 10 % NaOH could not be demolded due to insufficient strength gain. By comparison, only when 20 % NaOH was incorporated, the UCS of SEDS with 20 % NaOH is higher than that of CDS at all curing ages. Compared with CDS, the UCS of 7-, 28-, 60-, and 90-d SEDS containing 20 % NaOH exhibits 66.9 %, 79.4 %, 64.9 % and 40.4 % stronger, respectively. Fig. 5b presents the strength evolution of SSCP-stabilized DS (SPDS) against NaOH content, and increasing NaOH content results in the strength increase of SPDS. With increasing NaOH content to over 15 %, the UCS of SPDS at various curing ages is higher than that of CDS. The UCS of SSCD-stabilized DS (SDDS) versus NaOH content is shown in Fig. 5c; the UCS enhances firstly and then weakens with increasing NaOH content, and reaches the maximum at the NaOH content of 15 %. Thus, the optimum NaOH content for SDDS is 15 %. Although the UCS of SDDS decreases after adding 20 % NaOH, it remains higher than that of CDS. Through quantitative comparison, the highest 7-, 28-, 60- and 90-d UCS values of SDDS are 38.4 %, 39.8 %, 56.4 % and 38.8 % higher than that of CDS, respectively.

From the above observations, it can be obtained that using NaOH as an alkali-activator for the GGBS-EMR/PG/DG binary binder to prepare SSC is feasible and can effectively improve the stabilization efficiency on DS. To achieve the same or higher stabilization efficiency as an equal amount of OPC, at least 15 % NaOH needs to be added as an alkali-activator for GGBS-EMR/PD/DG binary binder. It

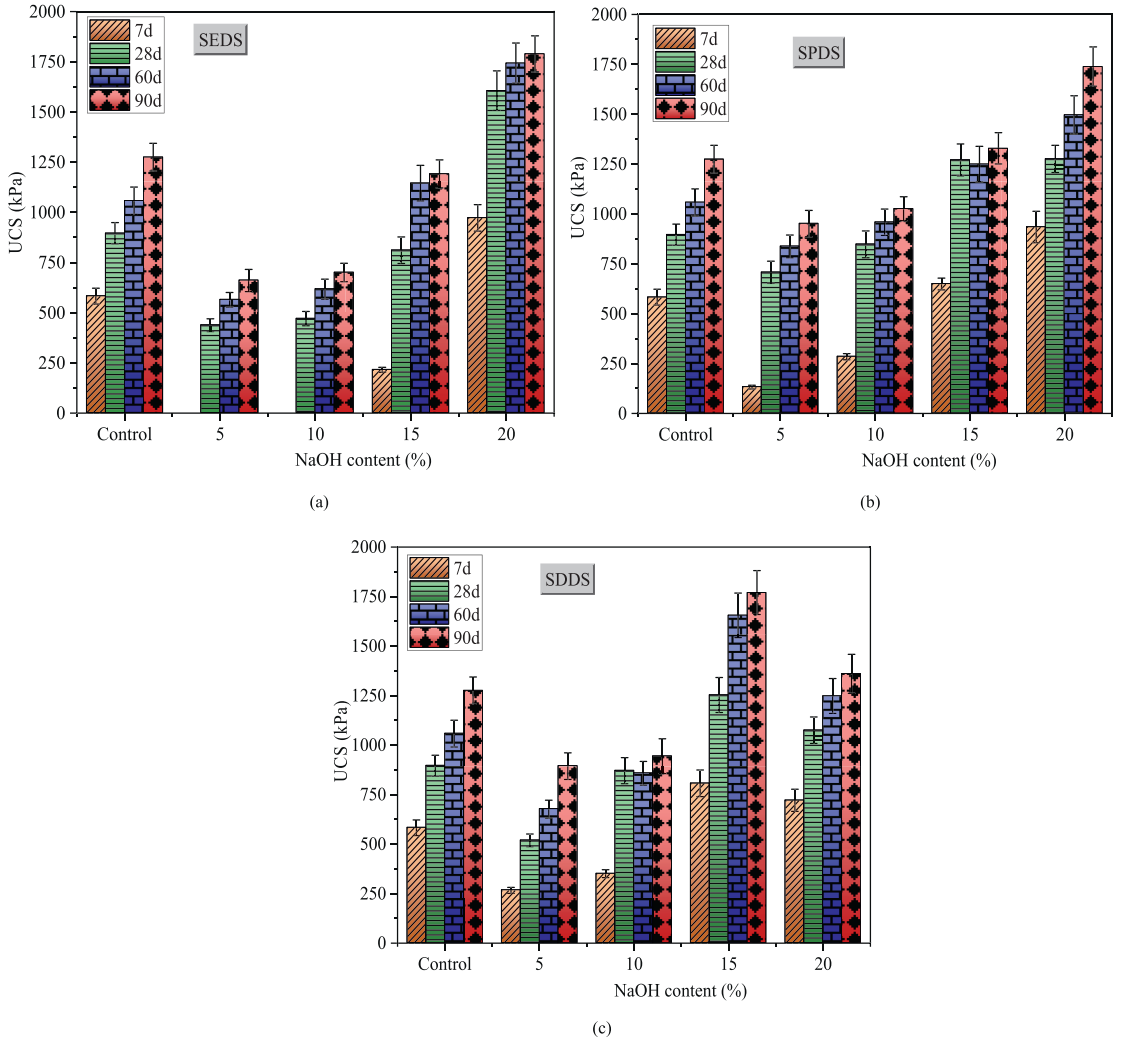

Fig. 5. Effect of NaOH content on the strength development of (a) SEDS, (b) SPDS, and (c) SDDS.

should be noted that the optimum NaOH content inside SEDS, SPDS, and SDDS is respectively 20 %, 20 %, and 15 %, exhibiting the difference in alkali-activator dosage. This is attributed to the difference in chemical compositions, especially CaO, Al_2O_3, and SO_3. The dosage of CaO and SO_3 in DG is higher than that in EMR and PG, while the Al_2O_3 in DG is lower than that in EMR and PG, as shown in Table 2. Under the existence of these active chemical components, adding suitable alkali-activator NaOH can contribute to the formation of cementitious products such as C-S-H, C-A-H and ettringite (AFt). However, the optimum dosage of NaOH is related to the chemical compositions inside GGBS-EMR/PG/DG, insufficient content of some active components may reduce the required NaOH demand. An insufficient NaOH content reduces the alkali-activation efficiency of GGBS, as the free water present in the DS dilutes the activator. This, in turn, hinders the generation of hydration products and the related cementation action of soil particles. Through alkali-activation, GGBS can hydrate like OPC and generate C-S-H and C-A-H gels. Simultaneously, the supply of Ca^{2+} and SO_4^{2-} from EMR/PG/DG promotes the formation of additional AFt. The formation of these cementitious gels is the primary driving force for the strength gain in SEDS, SPDS, and SDDS. Furthermore, AFt can also absorb a large amount of free water from DS, leading to an expansion effect, which can fill the micro-pores and form a dense interlocking structure within stabilized DS.

3.2. Effect of nano-modification

It has been determined that a minimum NaOH dosage of 15 % is required to activate the GGBS-EMR/PG/DG binary binder to achieve DS stabilization efficiency equivalent to or better than OPC. However, the addition of high dosage alkali-activator not only increases economic cost, but also increases the alkalinity of stabilized DS and associated environmental burdens. This is the reason why the 10 % NaOH was fixed for the subsequent experimental series. Therefore, controlling NaOH dosage and improving stabilization efficiency is a commendable win-win effect worthy of praise, and nano-modification was used as an effective approach to achieve this aim.

3.2.1. Effect of single NS-modification

Fig. 6 gives the influence of single NS-modification on the strength evolution of SEDS, SPDS, and SDDS, as well as the strength comparison of optimum NS-modified SSC-stabilized DS. Simultaneously, the UCS of CDS with 20 % OPC is also provided for comparison. The strength evolution of NS-modified SEDS (NS-SEDS) against NS content is given in Fig. 6a. It is clear that the UCS of NS-SEDS enhances with increasing NS content, and achieves the maximum at NS content of 10 %. Although incorporating NS can prominently enhance the strength development of SEDS, the UCS

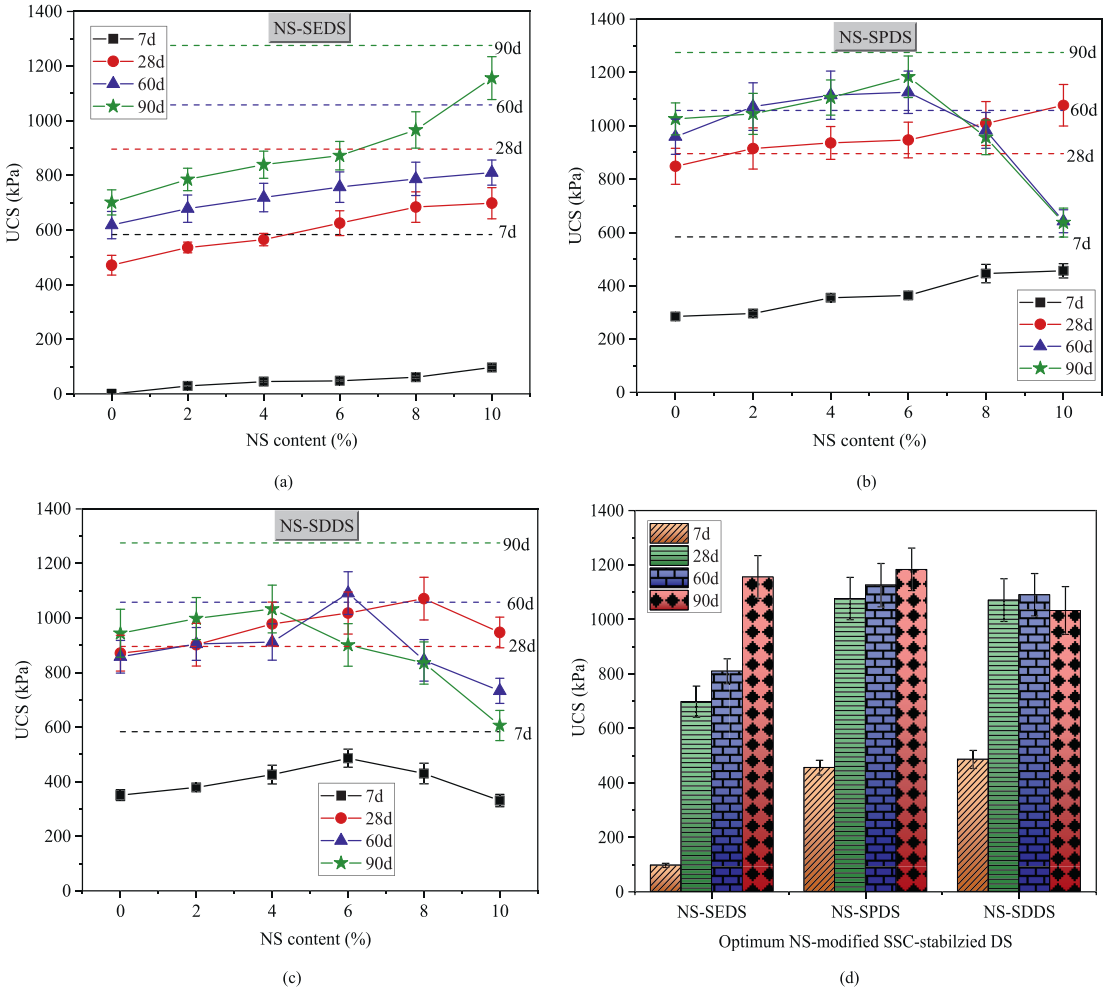

Fig. 6. Effect of single NS-modification on the strength development of NS-modified SEDS, SPDS, and SDDS.

at various curing ages is still lower than that of CDS. Fig. 6b presents the UCS of NS-modified SPDS (NS-SPDS) versus NS content. An optimum NS content for maximizing the strength of NS-SPDS is observed, which is 10 % for 7 d and 28 d of curing, and 6 % for 60 d and 90 d of curing, indicating that less NS is required for long-term strength gain of NS-CPDS. This is attributed to that excessive NS addition causes a local agglomeration effect inside NS-CPDS and weakens the strength gain. For early-term strength development of NS-CPDS, in addition to nano crystal nucleation effect, nano-filling effect also plays a significant role in the strength gain of NS-CPDS, which to some extent, compensates for the strength reduction caused by the local agglomeration effect. By comparison, the highest 28- and 60-d UCS of NS-CPDS exhibit a strength advantage over CDS, while the 7- and 90-d UCS of optimum NS-CPDS are respectively lower than that of CDS. The strength evolution of NS-modified SDDS (NS-SDDS) against NS content is illustrated in Fig. 6c, which first enhances and then decreases with increasing NS content. The highest 7-, 28-, 60-, and 90-d UCS are obtained under NS content of 6 %, 8 %, 6 % and 4 %, respectively, indicating that adding a suitable amount of NS can effectively enhance the strength development of NS-SDDS, while excessive NS actually has a side effect on the strength development of NS-SDDS. Furthermore, it can be found that the optimum NS content in NS-SDDS is clearly dependent on the curing time; the interaction between NS, SSCD, and DS under the influence of curing time is mainly responsible for this observation. The addition of NS promotes the further hydration of SSCD, and NS can be directly involved in the formation of cementitious products, especially C-S-H gel. With the extension of curing time, the active chemical components within the NS-SSCD gradually changed, resulting in an increase or decrease in the required optimum NS content. Compared with CDS, the optimum 28- and 60-d NS-SDDS exhibit a strength advantage, while the highest UCS of 7- and 90-d NS-SDDS is lower than that of CDS. The highest strength comparison of NS-SEDS, NS-SPDS, and NS-SDDS at various curing times is shown in Fig. 6d. The 7-d UCS of NS-SDDS is the highest, followed by NS-SPDS and NS-SEDS, while NS-SPDS reaches the highest UCS as the curing time exceeding 28 d.

3.2.2. *Effect of single NA-modification*

Fig. 7 shows the strength evolution of NA-modified SSC-stabilized DS versus NA content. The influence of NA content on the UCS of NA-modified SEDS (NA-SEDS) is shown in Fig. 7a, the 7-d NA-SEDS is difficult to demold, and consequently, no strength could be measured. The 28-, 60-, and 90-d UCS increases monotonically with increasing NA content until the highest strength is achieved at NA content of 10 %. Although the addition of NA improves the strength development of SEDS to some extent, the highest strength at various ages of NA-SEDS is lower than that of CDS. Fig. 7b presents the strength evolution of NA-modified SPDS (NA-SPDS) against NA content; the UCS first enhances and then decreases with increasing NA content. The highest 7-, 28-, 60-, and 90-d UCS

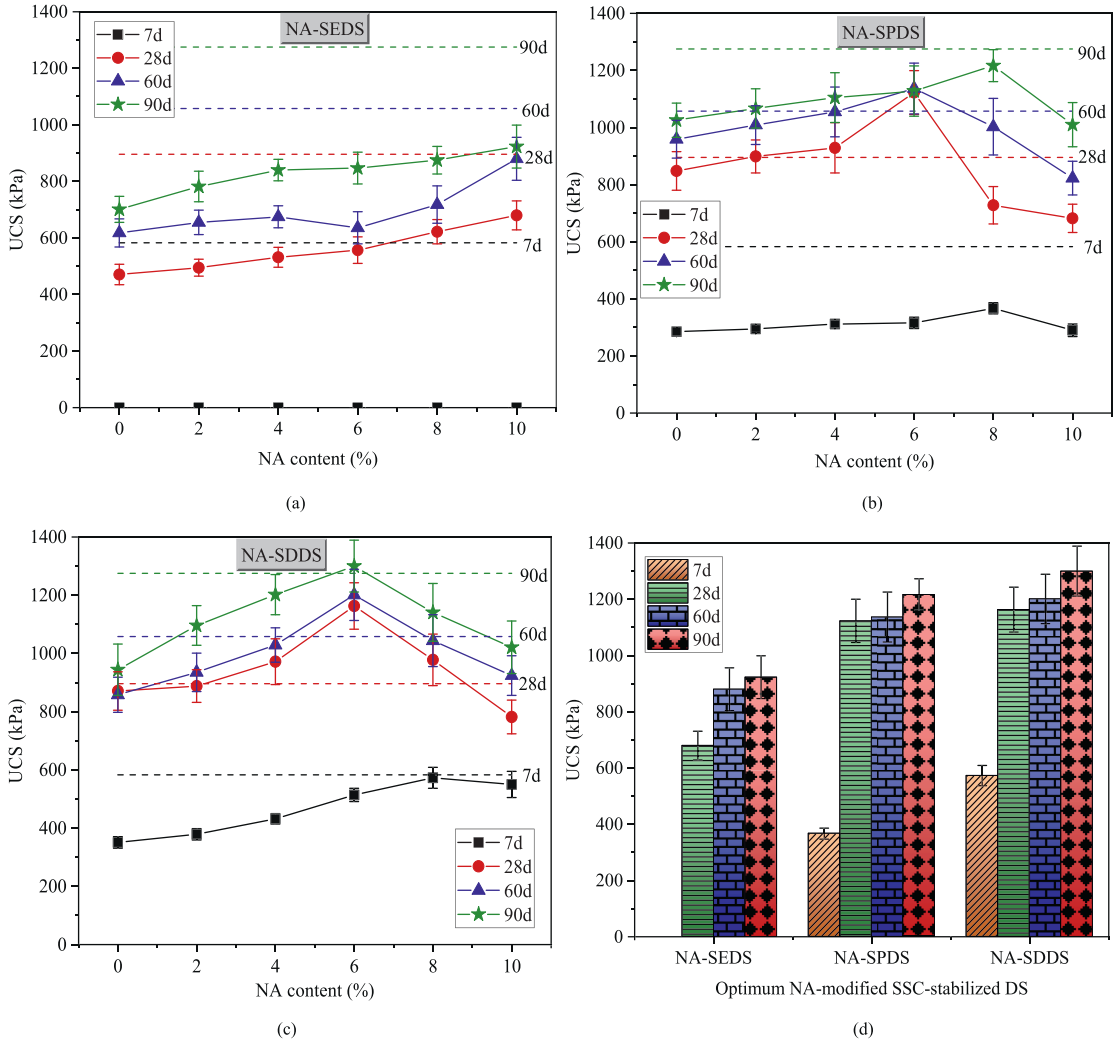

Fig. 7. Effect of single NA-modification on the strength development of NA-modified SEDS, SPDS, and SDDS.

of NA-SPDS are obtained under the NA content of 8 %, 6 %, 6 % and 8 %, respectively. By comparison, the 28- and 60-d UCS of optimum NA-SPDS are higher than that of CDS, while the 7- and 90-d UCS of optimum NA-SPDS are lower than that of CDS. Fig. 7c illustrates the effect of NA content on the strength development of NA-modified SDDS (NA-SDDS). An optimum NA content that maximizing the UCS of NA-SDDS is observed, which is respectively 8 %, 6 %, 6 % and 6 % for 7 d, 28 d, 60 d, and 90 d of curing. The 7-d UCS of optimum NA-SDDS is equivalent to that of CDS, while the 28-, 60-, and 90-d UCS of optimum NA-SDDS are respectively higher than that of CDS. This indicates that using 6 % NA-modified SSCD can fully replace OPC for DS stabilization. The strength comparison of optimum NA-SEDS, NA-SPDS, and NA-SDDS is shown in Fig. 7d. It is clear that the NA-SDDS has the highest strength at various curing ages, followed by NA-SPDS and NA-SEDS, respectively.

3.2.3. *Effect of composite NS/NA-modification*

It has been confirmed that adding a suitable amount of NS or NA can prominently improve the strength development of SEDS, SPDS, and SDDS. Furthermore, the NS and NA exhibit different nano-modification actions, which are mainly affected by the interaction between nanomaterials, SSC, and DS. To investigate the coupling nano-modification action between NS and NA on the strength development of three types of SSC-stabilized DS, under the addition of 6 % nanomaterials, the effect of composite NS/NA with various mass ratios (NS/NA) on the UCS of three types of nano-modified SSC-stabilized DS is shown in Fig. 8, and the corresponding UCS of single NS- and NA-modified SSC-stabilized DS is also listed as a comparison. The strength evolution of NS/NA-modified SEDS (NS/NA-SEDS) versus NS/NA is given in Fig. 8a, which first enhances and then decreases with increasing NS/NA, and achieves the highest under the NS/NA of 7/3. By comparison, the UCS of optimum NS/NA-SEDS at various curing ages is greater than that of NS-SEDS and NA-SEDS, indicating that composite NS/NA has better efficiency than single NS and NA. Furthermore, the nano-coupling action effect between NS and NA is observed within the composite system. Similar observations are evident in Fig. 8b and c, where the optimum NS/NA of 3/7 is obtained for the strength evolution of NS/NA-modified SPDS (NS/NA-SPDS) and NS/NA-modified SDDS (NS/NA-SDDS) versus NS/NA. Furthermore, the strength improvement induced by optimum NS/NA-modification is higher than that caused by single NS- and NA-modification. The optimum NS/NA in NS/NA-SEDS, NS/NA-SPDS, and NS/NA-SDDS is respectively 7/3, 3/7, and 3/7, and the composite NS/NA exhibits higher nano-modification efficiency than single nano-modification. Fig. 8d presents the strength comparison of optimum NS/NA-SEDS, NS/NA-SPDS, and NS/NA-SDDS, and the corresponding strength at various curing ages of CDS is also given as a

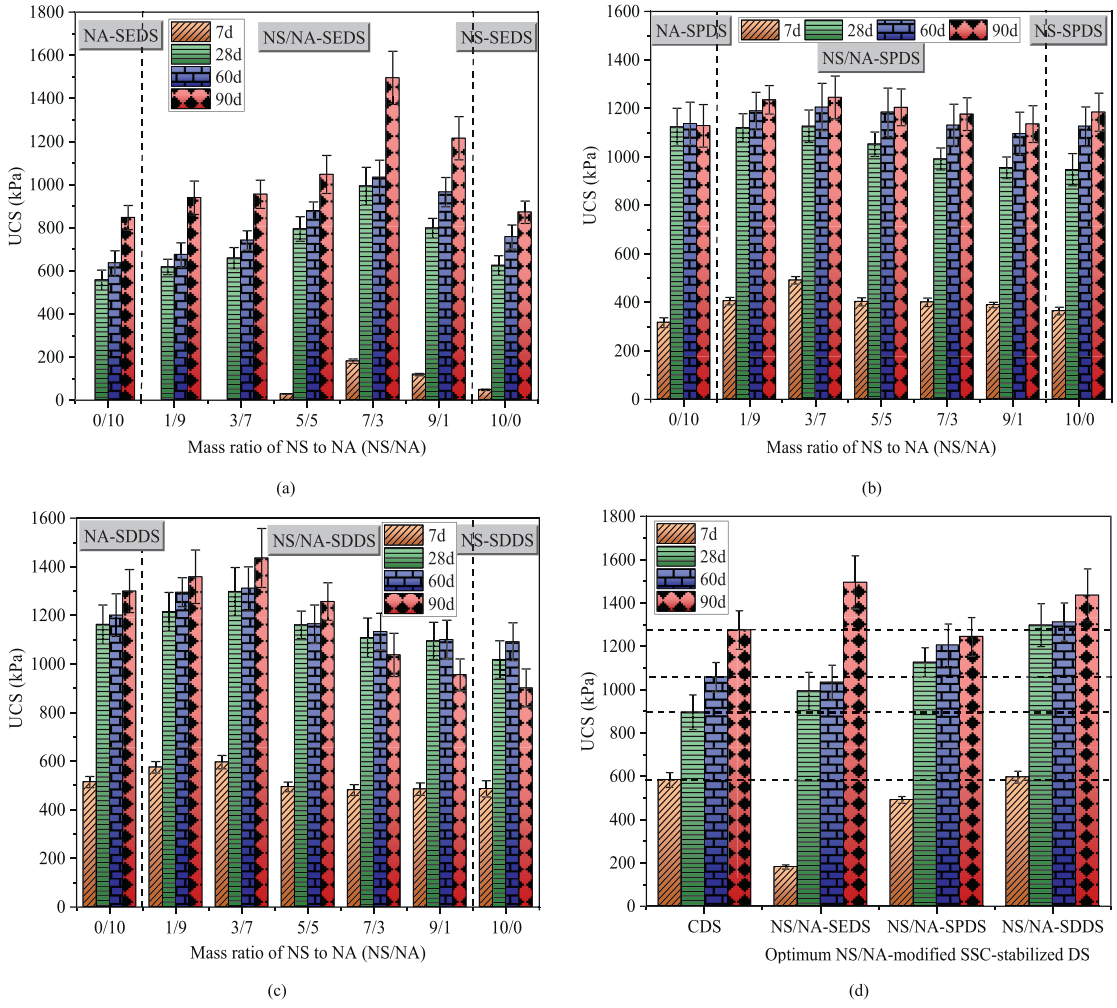

Fig. 8. Effect of composite NS/NA-modification on the strength development of NS/NA-modified SEDS, SPDS, and SDDS.

comparison. The 90-d UCS of NS/NA-SEDS is the highest, followed by NS/NA-SDDS and NS/NA-SPDS, respectively. However, the 7-, 28-, and 60-d UCS of NS/NA-SDDS are the highest, followed by NS/NA-SPDS and NS/NA-SEDS, respectively. By comparison, the 7-d UCS of CDS is higher than that of NS/NA-SEDS and NS/NA-SPDS, but slightly lower than that of NS/NA-SDDS. In addition, except for the 28-d UCS of NS/NA-SEDS, the 28-, 60-, and 90-d UCS of three types of SSC-stabilized DS exhibit a strength advantage over that of CDS. Therefore, using the optimum composite NS/NA as the helper of three types of SSC (SSCE, SSCP, and SSCD) can fully replace OPC in DS stabilization.

3.3. Leaching toxicity

The environmental risk evaluation of typical 28-d SEDS, NS-SEDS, NA-SEDS, and NS/NA-SEDS is significant for their further application in practical engineering, due to the presence of heavy metals and pollutants in EMR. Based on HJ/T 299-2007 (2007), the sulfuric acid & nitric acid method was used to determine the leaching toxicity of various heavy metals and ammonia nitrogen. The leaching results of raw EMR, SEDS, and optimum NS-, NA, and NS/NA-SEDS are shown in Table 5, and the limits of GB 5085.3-2007 (2007) and GB 8978-1996 (1996) are also given as a comparison. The leaching concentrations of heavy metal Mn and NH_4^+-N in EMR are much higher than the limitations of GB 8978-1996 (1996) and GB 5085.3-2007 (2007). Furthermore, the leaching concentrations of Zn, Cr, and Cu from EMR also exceeded the limits of GB 8978-1996 (1996). However, the leaching concentrations of various heavy metals and NH_4^+-N from pure SEDS, and NS-, NA-, and NS/NA-SEDS are far below the standard limits, with some heavy metals being undetectable. This was attributed to the fact that the heavy metals in raw EMR were effectively physically sealed and chemically fixed via the interaction between cementitious products and heavy metals. Furthermore, the NH_4^+-N was susceptible to migration and transformation during the hydration reaction process. This further indicates that using EMR as a raw material to prepare SSCE can not only recycle EMR, but also mitigate its environmental risks. Therefore, the SEDS and optimum nano-modified SEDS can be directly utilized as reclaimed engineering soils without considering environmental concerns.

3.4. XRD analysis

The crystalline phases for pure and nano-modified SEDS, SPDS, and SDDS at 28 d are given in Fig. 9. Based on the diffraction patterns, the detected mineral phases are mainly derived from two sources: DS itself and the hydration products of SSC. The minerals detected from DS include quartz [SiO_2], kaolinite [$Al_2(Al-Si_3O_{10})(OH)_2$], Illite [$KAl_2(AlSi_3O_{10})(OH)_2$], Plagioclase [$Na(Al-Si_3O_8)$-$Ca(Al_2Si_2O_8)$], and Calcite ($CaCO_3$), indicating that the

Table 5
Leaching results of raw material EMR, SEDS, and optimum nano-modified SEDS.

Pollutant	Concentration (mg/L)							
	Pb	Zn	Cr	Cd	Cu	As	Mn	NH^{4+}-N
EMR	0.308	4.084	0.654	0.031	0.685	0.015	2213	132.2
SEDS	0.021	ND	0.016	ND	0.008	0.009	ND	0.59
NS-SEDS	0.009	ND	0.008	ND	0.009	ND	ND	0.47
NA-SEDS	ND	ND	ND	ND	0.003	0.005	ND	0.19
NS/NA-SEDS	ND	ND	ND	ND	0.003	ND	ND	0.07
GB 8978-1996 (1996)	1	2	0.5	0.1	0.5	0.5	2	15
GB 5085.3-2007 (2007)	5	100	5	1	100	5	–	–

Note: ND means not detected.

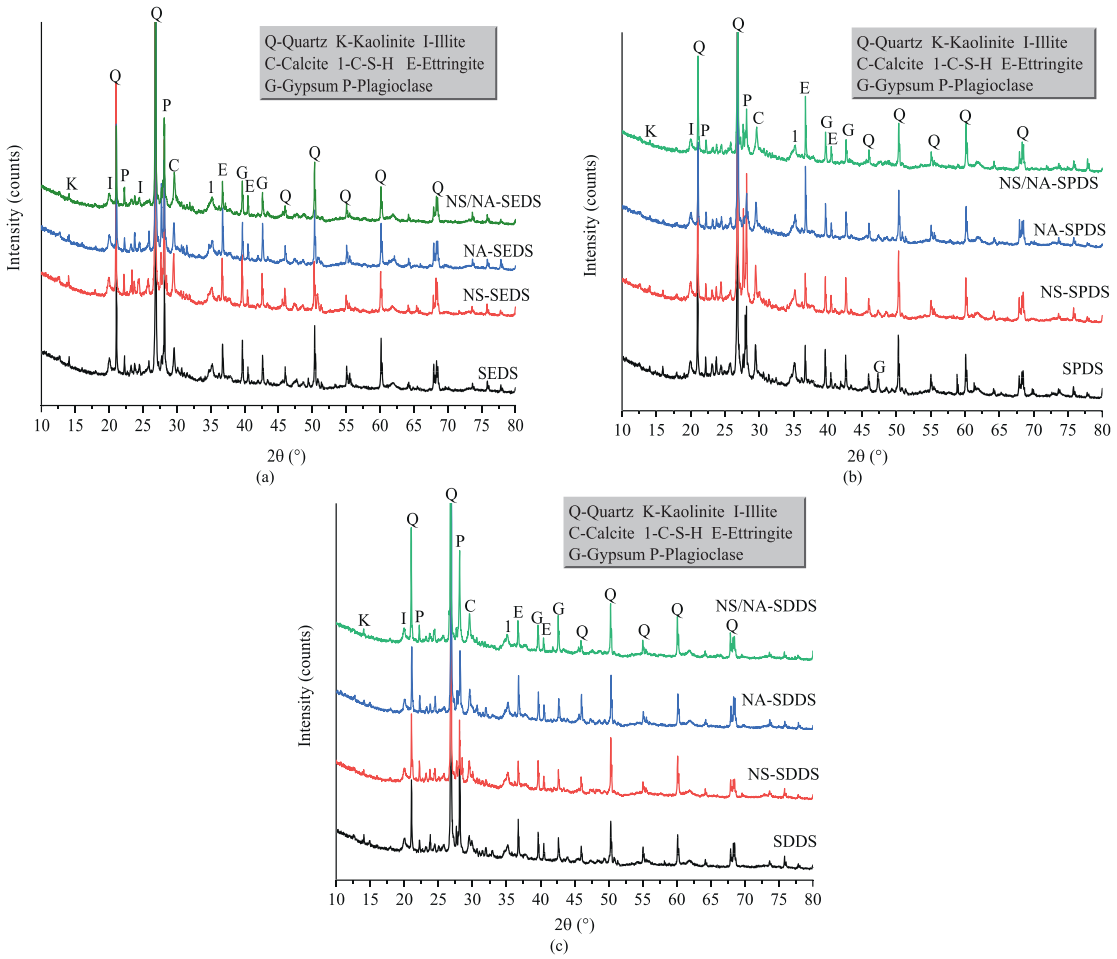

Fig. 9. XRD patterns of typical 28-d SEDS, SPDS, and SDDS with optimum single and composite nano-modifications.

chemical stabilization process has an insignificant effect on the mineral phases inside DS. In other words, the minerals from DS itself exhibits relatively high stability during interaction with nanoparticles, SSC, and soil particles. The hydration products of SSC detected are C-S-H gel and ettringite [$Ca_6Al_2(SO_4)_3(OH)_{12}{\cdot}32H_2O$], indicating that the main hydration products of SSC are C-S-H gel and ettringite, and similar analysis results were also reported by Kang et al. (2024). Under alkali-activation by NaOH, the vitreous body in GGBS was destroyed, releasing dissolved OH^-, Ca^{2+}, Al^{3+}, and SO_4^{4-}. Subsequently, the incorporation of three sulfate wastes (EMR, PG, and DG) provided SO_4^{2-} and additional Ca^{2+}. These ions react with each other and formed C-S-H, C-A-H, and ettringite, and then contribut to the formation of the structural network. Noting that the C-A-H gel was not clearly detected by XRD analysis. One reason is that its peaks may overlap with those of other minerals, and another is consumed during the formation of ettringite.

The effect of incorporating optimum NS, NA, and NS/NA on the mineral phases of SEDS, SPDS, and SDDS is further analyzed. Apart from nano-filling and crystal nucleation effects, NS and NA can even be directly involved in the formation of cementitious gels. However, the addition of NS has no significant effect on the diffraction peak intensity of C-S-H gel, which may be related to the insufficient concentration of $Ca(OH)_2$. By comparison, adding NA significantly improves the diffraction peak intensity of ettringite. This is because, on the one hand, Al_2O_3 reacted directly with SO_4^{2-},

Ca^{2+}, and OH^- to produce ettringite, and on the other hand, NA contributed to the conversion of C-A-H gel to ettringite. It has been reported that C-S-H and ettringite gels are the main cementitious products of SSC, and NS and NA are confirmed to be respectively beneficial for the formation of C-S-H and ettringite gels. Thus, compared with single NS and NA, composite NS/NA provides the greatest enhancement to the strength development of SEDS, SPDS, and SDDS, as illustrated in Fig. 8. Furthermore, the detection of gypsum ($CaSO_4{\cdot}2H_2O$) indicates that it was not completely consumed, which is beneficial for preventing the conversion of ettringite to monosulfoaluminate (AFm) and the associated strength reduction.

3.5. SEM analysis

Typical SEM images of pure and nano-modified SEDS, SPDS, and SDDS at 28 d are presented in Figs. 10–12. Fig. 10a–d presents the microstructure of pure SEDS, optimum NS-, NA-, and NS/NA-modified SEDS, indicating that for pure SEDS shown in Fig. 10a, obvious micro-pores and needle-shaped AFt are distributed among the soil particles. Furthermore, AFt, other products, and soil particles intertwine together to form cemented soil particles, which serves as the basis for the strength gain of SEDS. Under the optimum NS-modification, as shown in Fig. 10b, the amorphous cluster C-S-H gel is clearly observed, indicating that incorporating NS accelerates the hydration degree and produces more C-S-H gel. The synergistic reinforcement effect of C-S-H gel and Aft leads to the formation of a denser cemented soil matrix. Fig. 10c presents the microstructure of optimum NA-SEDS; some micro-pores may be caused by the excessive formation of AFt due to the expansion reaction (Xu and Yi, 2021). This suggests that incorporating NA not only accelerates the hydration process of SSC but also contributes to the formation of more AFt. The microstructure of optimum NS/NA-SEDS is shown in Fig. 10d, compared with pure and optimum single nano-modified SEDS, a dense cemented soil matrix with few visible micro-pores was observed. This indicates that composite NS/NA-modification is beneficial for the formation of an extensive crystal interlocking structure inside SDES and contributes to the highest strength development, aligning with the strength and XRD results.

Fig. 11a presents the microstructure of pure SPDS, where abundant needle-shaped AFt and columnar gypsum were observed. Compared with the microstructure of pure SEDS shown in Fig. 10a, the formation of more AFt mainly is the primary reason for the strength advantage of SPDS over SEDS (Fig. 5). After NS-modification, a reticular C-S-H gel is clearly observed, leading to the formation of a dense cemented soil matrix within NS-SPDS, as shown in Fig. 11b. By comparison, more AFt is found in NA-SPDS, as shown in Fig. 11c, confirming that the incorporation of NS and NA is respectively beneficial for the formation of C-S-H gel and AFt. The microstructure of NS/NA-SPDS is shown in Fig. 11d, and amorphous cluster C-S-H gel, micro-pores, and cemented soil particles are clearly observed. By comparison, the microstructure of NS/NA-SPDS is more compact than that of the pure and single nano-modified SPDS.

Fig. 12a presents the microstructure of pure SDDS, where micro-pores and needle-shaped AFt are clearly observed. The AFt is embedded within soil particles, forming cemented soil particles. By adding an optimum amount of NS, the microstructure of NS-SDDS is given in Fig. 12b, abundant reticular C-S-H gels appear and are interwoven with AFt. Furthermore, pronounced micro-pores are also observed, which weaken the strength gain of NS-SDDS. The microstructure of NA-SDDS is illustrated in Fig. 12c, which is similar to that of NS-SDDS shown in Fig. 12b. The microstructure of NS/NA-SDDS is shown in Fig. 12d, where the massive reticular cluster C-S-H gel is found, forming a denser

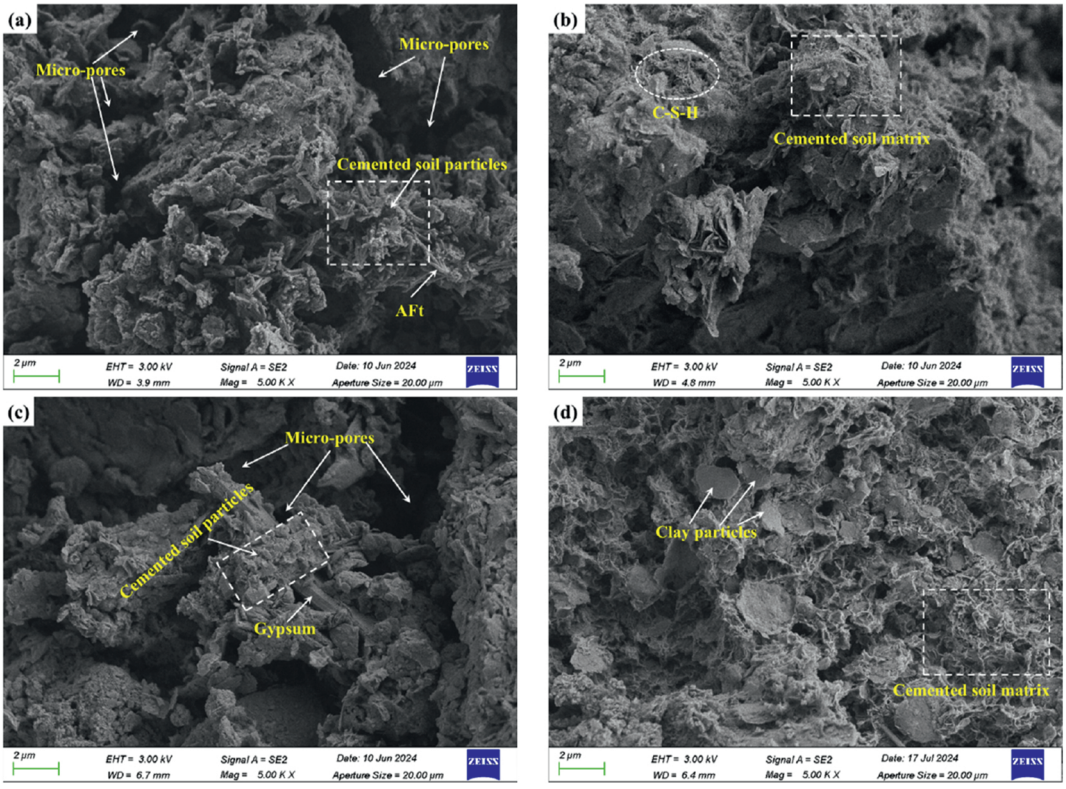

Fig. 10. SEM micrographs of typical 28-d stabilized DS: (a) pure SEDS, and optimum (b) NS-SEDS, (c) NA-SEDS, (d) NS/NA-SEDS.

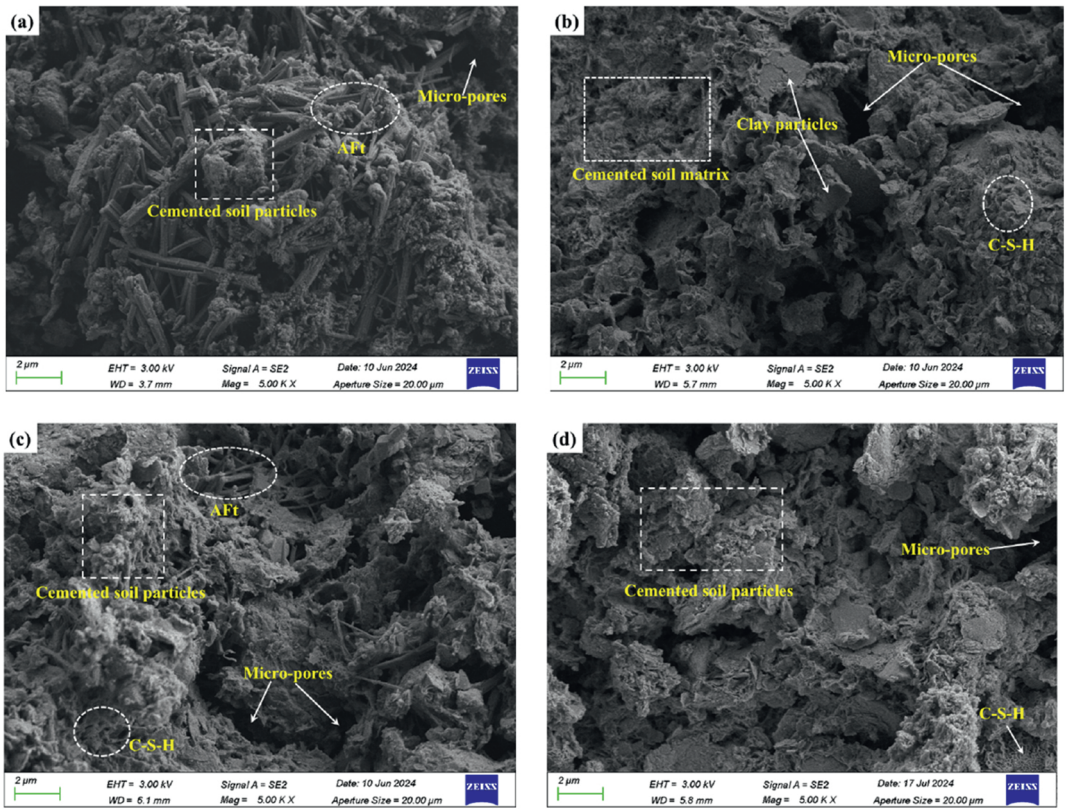

Fig. 11. SEM micrographs of typical 28-d stabilized DS: (a) pure SPDS, and optimum (b) NS-SPDS, (c) NA-SPDS, (d) NS/NA-SPDS.

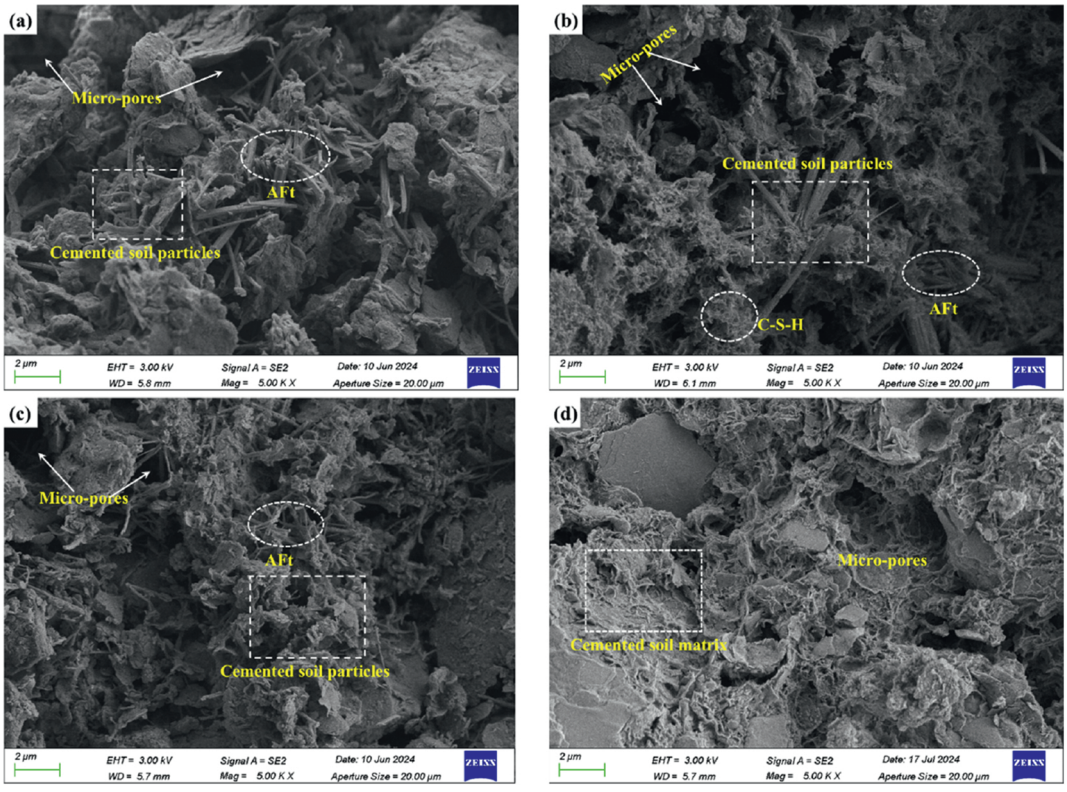

Fig. 12. SEM micrographs of typical 28-d stabilized DS: (a) pure SDDS, and optimum (b) NS-SDDS, (c) NA-SDDS, (d) NS/NA-SDDS.

cemented soil matrix. The NS/NA-SDDS exhibits a denser and more compact microstructure than pure SDDS and single nano-modified SDDS; a result mainly attributed to the nano-coupling effect.

Based on the above observations and analysis, three key findings can be achieved. Firstly, the microstructure of SEDS, SPDS, and SDDS varies, a difference stemming from the type of sulfate solid waste and associated chemical components inside SSC. Secondly, Nano-modification can effectively densify the microstructure, and NS and NA mainly contribute to the additional formation of C-S-H gel and AFt, respectively. Furthermore, compared with single NS- and NA-modification, the composite NS/NA-modification is more effective in forming a denser and more compact microstructure, thereby contributing to the highest strength gain.

3.6. TG-DTG analysis

The TG-DTG curves of 28-d stabilized DS samples (SEDS, SPDS, and SDDS) without and with nano-modification are given in Fig. 13, with typical minerals marked. All TG-DTG curves listed in Fig. 13a and b shows a similar evolution trend with increasing temperature, indicating that the mineral types inside pure and nano-modified stabilized DS are similar. Within the range of room temperature to 1000 °C, the DTG curves exhibit three main endothermic peaks. The first weight loss peak within 100 °C is highly likely caused by the dehydration of C-S-H gel and AFt. Sun et al. (2024) found that the weight loss in the 40 °C–280 °C corresponds to the loss of weak-bound water in C-S-H gel and ettringite. The weight loss between 400 °C and 500 °C may be attributed to the decomposition of kaolinite from DS and portlandite (CH) during the hydration process, as previously obtained by Li and Yi (2023). However, the CH was not obviously detected by XRD and SEM tests. In principle, the consumption rate of CH required for AFt generate is much faster than its generation rate, leading to its likely exhaustion. The weight loss peak at 600 °C–800 °C is mainly attributed to the decomposition of calcite (CaCO3). These conservations and analyses further confirm that the main hydration products in both pure and nano-modified stabilized DS samples are C-S-H gel and AFt. Fig. 13a shows that the weight loss associated with C-S-H gel and Aft is greatest for SPDS, followed by SDDS and SEDS, respectively. As shown in Fig. 13b, the weight loss of NS/NA-SEDS, NS/NA-SPDS, and NS/NA-SDDS shows no significant difference. The TG-DTG analysis results are consistent with the strength development, XRD, and SEM results.

4. Discussion

4.1. Chemical activation mechanism

In this study, three kinds of low-carbon SSC (SSCE, SSCP, and SSCD) were prepared by synthesizing alkali-activator NaOH, GGBS, and three types of sulfate solid wastes (EMR, PG, and DG), and they were used to stabilize DS. The results show that adding a suitable amount of NaOH can significantly enhance the stabilization efficiency of SSC. The strength development of the stabilized DS is primarily attributed to the interaction between NaOH, GGBS, and sulfate solid waste, an effect that is essentially the synergistic activation of GGBS by alkali and sulfate.

The NaOH reacted with water to form a strong alkaline solution and released OH^- (see Eq. (1)), which facilitated the structural dissociation of metastable vitreous phase in GGBS. This process led to the gradual release of Ca^{2+}, Al^{3+}, and active silica tetrahedral oligomers (SiO_4^{4-}). When the sulfate solid wastes were mixed with water, they all dissolved and released Ca^{2+} and SO_4^{2-}. These ions gradually accumulated over time and reacted with each other in solution, leading to the nucleation, growth, and overlapping of hydration products, which formed the cemented network structure. Specifically, the free Ca^{2+} reacted with SiO_4^{4-} to produce C-S-H gel (see Eq. (2)). Simultaneously, the Al^{3+} reacted with Ca^{2+} to produce C-A-H gel (see Eq. (3)). Under the supply of SO_4^{2-} from sulfate solid wastes, the Ca^{2+} and Al^{3+} were further consumed to produce AFt (see Eq. (4)). This process further accelerated the hydration of GGBS and maximized its potential activity. Furthermore, the C-A-H gel produced in Eq. (3) is further consumed by SO_4^{2-} to produce additional AFt (see Eq. (5)). This likely explains why the C-A-H gel was not detected by XRD tests. In general, these hydration products contributed to the strength gain of SSC-stabilized DS. Especially for stabilizing high water content DS, the formation of AFt can consume a large amount of free water, thus providing an expansion filling effect. However, the excessive production of AFt and its induced expansion effect also had a side effect on the strength development of SSC-stabilized DS. The possible interaction mechanism between GGBS, alkali activator NaOH, and sulfate solid wastes is shown in Fig. 14. Therefore, the main hydration products of SSC are C-S-H gel and AFt, contributing to the strength development of the three kinds of SSC-stabilized DS. It should be noted that the stabilization efficiency of SSCE, SSCP, and SSCD is different; which is attributed to the difference in

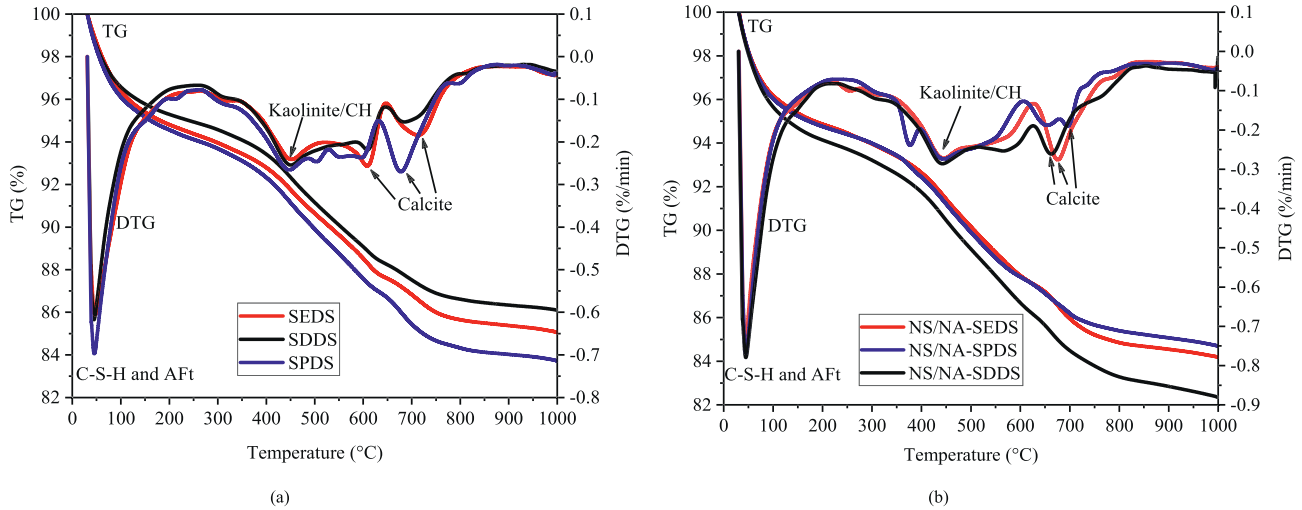

Fig. 13. TG/DTG curves of (a) pure SEDS, SPDS, and SDDS, (b) optimum NS/NA-SEDS, SPDS, and SDDS.

Fig. 14. The interaction mechanism between GGBS, alkali activator NaOH, and sulfate solid wastes.

the chemical components of EMR, PG, and DG.

$$NaOH + H_2O \rightarrow Na^+ + OH^- \quad (1)$$

$$SiO_4^{4-} + Ca^{2+} + H_2O \rightarrow \text{C-S-H gel} \quad (2)$$

$$Al^{3+} + Ca^{2+} + H_2O \rightarrow \text{C-A-H gel} \quad (3)$$

$$Al^{3+} + Ca^{2+} + SO_4^{2-} + H_2O \rightarrow \text{AFt} \quad (4)$$

$$\text{C-A-H gel} + SO_4^{2-} + H_2O \rightarrow \text{AFt} \quad (5)$$

4.2. Nano-modification mechanism

The results of this study imply that nano-modification can effectively improve the stabilization efficiency of three kinds of SSC on DS, and compared with single NS or NA, the composite NS/NA exhibits better nano-modification efficiency. Three nano-modification actions were mainly responsible for this improvement in stabilization efficiency. Firstly, the nano-filling effect effectively reduces the micro-pores within cemented soil particles (Lang et al., 2023), thus improving the compactness of SSC-stabilized DS. Secondly, nano-induced activation effect can further promote the hydration process of binder, and thus produce additional cementitious gels (Wang et al., 2020). For example, the NS and NA used in this study, respectively, involved the additional formation of C-S-H gel and AFt by consuming $Ca(OH)_2$ and $CaSO_4$; this reaction process contributed to the further hydration of SSC. Thirdly, the nano-nucleation effect can provide more active targets for the formation of hydration products, transforming them from a loose needle-cluster-like structure to a denser, uniform-stable network structure. Furthermore, nanoparticles can absorb double-layer water and form a viscous gel among soil particles, thereby improving the cementation strength among soil particles (Changizi et al., 2022). Therefore, it can be achieved that the formation of more C-S-H gel and AFt improved the stabilization efficiency of SSC, which was mainly induced by NS- and NA-modification actions, respectively. The micro-mechanism model for nano-modified SSC-stabilized DS is given in Fig. 15.

4.3. Engineering application prospects and future work

In this study, three kinds of nano-modified low-carbon SSC were prepared and used for stabilizing DS, offering two main benefits. First, the 28-d UCS of all three optimum NS/NA-modified SSC-stabilized DS exceeded 1 MPa (see Fig. 8), meeting the minimum strength requirement for subgrade materials, based on T/CECS 737-2020 (2020). Therefore, the NS/NA-modified SSC-stabilized DS can be used as sustainable subgrade materials, thereby saving non-renewable soil and rock resources during road construction. Second, it provides an effective consumption pathway for industrial solid wastes (including GGBS, EMR, PG, DG) and waste DS. The collaborative resource utilization of industrial solid wastes and DS as reclaimed engineering soils can not only reduce the environmental burdens caused by their storage or landfill, but also reduce the dependence on traditional binders such as Portland cement and lime.

However, some disadvantages regarding the application of nano-modified SSC for DS stabilization pose significant challenges. Firstly, the excessive use of high alkalinity NaOH also causes environmental pollution to the surrounding soil and water, as well as the high CO_2 emission. Secondly, the high price of NaOH and nanomaterials will inevitably increase the engineering cost of stabilizing DS, limiting the widespread application of this technology. It is expected that this issue will be effectively alleviated with advances in production technologies for NaOH and nanomaterials. Furthermore, the basic properties, especially chemical components of raw materials (including GGBS, EMR, PG, and DG), may vary depending on the source and production process, significantly affecting the hydration and hardening performances and associated stabilization efficiency on DS. For example, as sulfate solid wastes, the difference in chemical components of EMR, PG, and DG was mainly responsible for the difference in hydration-cementation ability and related stabilization efficiency of the three kinds of SSC (SSCE, SSCP, and SSCD). It is recommended that the mineral component reconstruction, pre-treatment, and impurity removal processes may be the potential solutions.

Based on the advantages and disadvantages stated above, future work should focus on three aspects. Firstly, additional

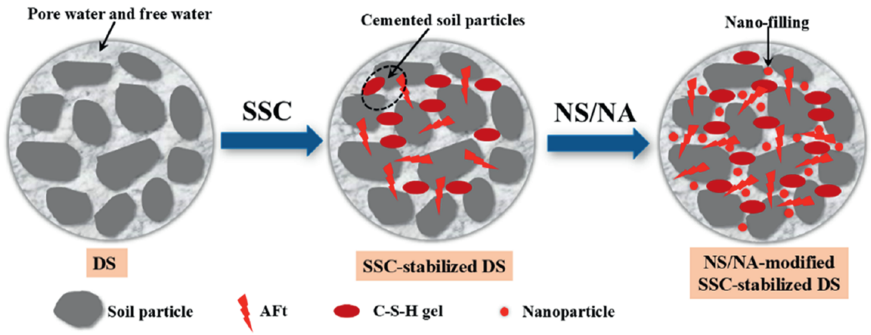

Fig. 15. The micro-mechanism model for nano-modified SSC-stabilized DS.

research is needed to quantitatively evaluate the economic benefit and carbon emission reduction of using SSC in DS stabilization, compared with traditional Portland cement. Secondly, the durability of nano-modified SSC-stabilized DS under complex environmental conditions, such as chemical erosion, dry-wet and freeze-thaw cycles, should be investigated, which is essential for the subsequent engineering applications. Lastly, due to the price and environmental concerns caused by alkali-activator NaOH, other single or composite industrial solid waste alkali activators, such as carbide slag and red mud, are encouraged to replace NaOH for full solid waste SSC preparation and DS stabilization.

5. Conclusions

In this study, three types of full solid waste supersulfated cement (SSCE, SSCP, and SSCD) were synthesized by NaOH-activated GGBS and sulfate solid wastes (EMR, PG, and DG), which were used to stabilize DS with high water content, and NS and NA were also used as single and composite nano-modifiers to further improve stabilization efficiency. The effect of NaOH-activation and nano-modification action on the strength development of stabilized DS was evaluated via UCS tests. The micro-mechanisms underlying this strength development of stabilized DS were elucidated through XRD, SEM, and TG-DTG analyses. Furthermore, the leaching toxicity of SSCE-stabilized DS was investigated to evaluate the environmental risks. The key conclusions are as follows.

(1) NaOH is an effective activator for the GGBS-EMR/PG/DG binary cementitious system, significantly improving the cementation ability of SSC and its stabilization efficiency for DS. The strength of SSCE-stabilized DS (SEDS) and SSCP-stabilized DS (SPDS) increased monotonically with increasing NaOH content, while the highest strength of SSCD-stabilized DS (SDDS) was achieved under NaOH content of 15 %.
(2) Nano-modification can effectively enhance the stabilization efficiency of three kinds of SSC on DS. Adding a suitable amount of single NS and NA can prominently increase the strength development of stabilized DS, while the optimum dosage of NS and NA varies depending on the type of SSC and curing time. The optimum NA-modified SSCD-stabilized DS exhibited a strength advantage over OPC-stabilized DS. Composite nano-modification outperforms single nano-modification in improving stabilization efficiency. For SEDS, SPDS, and SDDS, the optimum mass ratios of NS to NA were 7:3, 3:7, and 3:7, respectively.
(3) Although EMR contains heavy metals and ammonia nitrogen, its use as a raw material for preparing SSC poses no significant environmental risks. The leaching results of SEDS, optimum NS-, NA-, and NS/NA-SEDS are far below the standard limits, indicating that SEDS and nano-modified SEDS can be directly utilized as reclaimed engineering soils without environmental concerns.
(4) The C-S-H gel and AFt are the main hydration cementitious products in the three SSC-stabilized DS and are primarily responsible for the strength development. NS and NA respectively promote the additional formation of C-S-H gel and AFt, an effect attributed to their direct participation in the formation of these hydration products. Composite NS/NA-modification was more effective in forming a denser and more compact microstructure within stabilized DS, thereby facilitating the highest strength development.
(5) The mechanisms of chemical activation and nano-modification affecting the cementation ability and associated stabilization efficiency on DS were respectively clarified. Correspondingly, the interaction between GGBS, alkali activator NaOH, and sulfate solid wastes, as well as the micro-mechanism model for nano-modified SSC-stabilized DS, were respectively proposed. Furthermore, the advantages and disadvantages of using nano-modified SSC in DS stabilization were discussed, and the future work was highlighted.

CRediT authorship contribution statement

Lei Lang: Writing – original draft, Project administration, Methodology, Investigation, Funding acquisition, Conceptualization. **Dongxing Wang:** Validation, Methodology, Investigation, Data curation. **Bing Chen:** Validation, Resources, Methodology, Investigation. **Desheng Li:** Methodology, Investigation. **Linlin Gu:** Writing – original draft, Supervision, Methodology, Investigation.

Declaration of competing interest

The authors declare that they have no known competing financial interests or personal relationships that could have appeared to influence the work reported in this paper.

Acknowledgments

This study was supported by the National Natural Science Foundation of China (Grant No. 42307232), the Science Fund for Distinguished Young Scholars of Hubei Province (Grant No. 2024AFA051), and the National Natural Science Foundation of China (Grant No. U24A20183).

References

ASTM D2166-16, 2016. Standard Test Method for Unconfined Compressive Strength of Cohesive Soil. ASTM International, West Conshohocken, PA.
Aksu, G., Eskisar, T., 2023. The geomechanical properties of soils treated with nanosilica particles. J. Rock Mech. Geotech. Eng. 15, 954–969.
Cao, W., Lv, X., Ban, J., Lu, J.-X., Liu, Z., Chen, Z., Poon, C.S., 2024. High-efficient stabilization and solidification of municipal solid waste incineration fly ash by synergy of alkali treatment and supersulfated cement. Environ. Pollut. 355, 124261.
Chang, S., Gao, F., Wang, L., Jin, Q., Liu, S., Wan, L., 2024. Deterioration mechanism of supersulfated cement paste exposed to sulfate attack and combined acid-sulfate attack. Constr. Build. Mater. 414, 134978.
Changizi, F., Ghasemzadeh, H., Ahmadi, S., 2022. Evaluation of strength properties of clay treated by nano-SiO2 subjected to freeze-thaw cycles. Road Mater. Pavement Des. 23 (6), 1221–1238.
Chen, T., Wang, L., He, B., Peng, X., Nie, X., Ma, F., Han, P., Bai, X., 2024a. Study on the solidification/stabilization of cadmium-contaminated soil by red mud-assisted blast furnace slag under excitation conditions. J. Clean. Prod. 435, 140505.
Chen, Z., You, N., Chen, C., Chen, L., Zhang, Z., Xu, W., Jia, Z., Zhang, Y., 2024b. The positive role of phosphogypsum in dredged sediment solidified with alkali-activated slag. Constr. Build. Mater. 442, 137627.
Chen, Q., Xie, K., Tao, G., Nimbalkar, S., Zhang, H., 2024c. Laboratory assessment of impact of nano-SiO2 on different soil types in onshore and offshore environment. Acta Geotech 19, 5065–5087.
Choobbasti, A.J., Samakoosh, M.A., Kutanaei, S.S., 2019. Mechanical properties soil stabilized with nano calcium carbonate and reinforced with carpet waste fibers. Constr. Build. Mater. 211, 1094–1104.
Dai, D., Lai, Z., Yu, H., Meng, T., Xu, Q., Li, J., Vandevyvere, B., Shen, H., 2024. Mechanical properties, microstructure, and mechanism of nanosilica-modified low-carbon magnesium silicate hydrate cement. J. Mater. Civ. Eng. 36 (11), 04024374.
GB 8978-1996, 1996. Integrated Wastewater Discharge Standard. Ministry of Environmental Protection (in Chinese).
GB 5085.3-2007, 2007. Identification Standards for hazardous wastes-identification for extraction toxicity. Ministry of Ecology and Environment of the People's Republic of China (in Chinese).
GB/T 50123-2019, 2019. Standard for Geotechnical Testing Method. Chinese Planning Press, Beijing, China (in Chinese).
Hossain, M.U., Wang, L., Chen, L., Tsang, D.C.W., Ng, S.T., Poon, C.S., Mechtcherine, V., 2020. Evaluating the environmental impacts of stabilization

and solidification technologies for managing hazardous wastes through life cycle assessment: a case study of Hong Kong. Environ. Int. 145, 106139.
HJ/T 299-2007, 2007. Solid waste-extraction Procedure for Leaching toxicity-Sulphuric Acid & Nitric Acid Method. Ministry of Ecology and Environment of the People's Republic of China (in Chinese).
Kang, Z., Zhang, J., Li, N., Lv, T., Yang, Y., Lu, J., 2024. Utilization of biochar as a green additive in supersulfated cement: properties, mechanisms, and environmental impacts. Constr. Build. Mater. 445, 137923.
Khodaparaast, M., Rajabi, A.M., Mohammadi, M., 2021. Mechanical properties of silty clay soil treated with a mixture of lime and zinc oxide nanoparticles. Constr. Build. Mater. 281, 122548.
Lang, L., Chen, B., Li, J., 2023. High-efficiency stabilization of dredged sediment using nano-modified and chemical-activated binary cement. J. Rock Mech. Geotech. Eng. 15, 2117–2131.
Lang, L., Li, J., Huang, X., Wang, P., Zhang, W., 2024a. Coupling effect of cement-stabilization and biopolymer-modification on the mechanical behavior of dredged sediment. J. Rock Mech. Geotech. Eng. 16, 3284–3298.
Lang, L., Li, J., Chen, X., Han, L., Wang, P., 2024b. Tensile strength behavior of cement-stabilized dredged sediment reinforced by polypropylene fiber. Front. Struct. Civ. Eng. 18 (3), 380–392.
Lang, L., Zhu, M., Pu, S., 2025. Recycling engineering sediment waste as sustainable subgrade material using ground granulated blast-furnace slag, electrolytic manganese residue and cement. Environ. Tehcnol. Inno. 37, 103969.
Li, W., Yi, Y., Puppala, A.J., 2022. Comparing carbide sludge-ground granulated blastfurnace slag and ordinary Portland cement: different findings from binder paste and stabilized clay slurry. Constr. Build. Mater. 321, 126382.
Li, W., Yi, Y., 2023. Estimating the optimum addition of carbide sludge for enhancing strength development of ground-granulated blast furnace slag-treated slurry based on initial pH. J. Mater. Civ. Eng. 35 (2), 04022400.
Li, S., Wang, D., Tang, C., Chen, Y., 2023. Optimization of synergy between cement, slag, and phosphogypsum for marine soft soil solidification. Constr. Build. Mater. 374, 130902.
Li, D., Lang, L., Dong, M., Hu, Z., 2025. Stabilization of dredged sediments containing humic acid with nano-modified ordinary Portland cement-sulphoaluminate cement. J. Soils Sediments 25, 1040–1055.
Liu, X., Hou, P., Chen, H., 2021. Effects of nanosilica on the hydration and hardening properties of slag cement. Constr. Build. Mater. 282, 122705.
Liu, H., Li, Q., Ni, S., Wang, L., Yue, G., Guo, Y., 2022. Effect of nano-silica dispersed at different temperatures on the properties of cement-based materials. J. Build. Eng. 46, 103750.
Liu, S., Zhang, R., Zheng, J., Xu, Z., 2023. Strength development behavior of cement-treated mud with emphasis on early-stage performance. Int. J. GeoMech. 23 (9), 04023144.
Ren, Z., Wang, L., Wang, H., Liu, S., Liu, M., 2023. Solidification/stabilization of lead-contaminated soils by phosphogypsum slag-based cementitious materials. Sci. Total Environ. 857, 159552.
Sun, Z., Nie, S., Zhou, J., Li, Hui, Chen, Z., Xu, M., Mu, R., Wang, Y., 2022. Hydration mechanism of calcium sulfoaluminate-activated supersulfated cement. J. Clean. Prod. 333, 130094.
Sun, Z., Chen, W.-B., Zhao, R.-D., Li, J.-S., Yin, Z.-Y., Yin, J.-H., Chen, Y.-G., 2024. Physicochemical properties of clayey deposits slurry treated by lime-activated ISSA and GGBS considering seawater salinity effect. Appl. Clay Sci. 248, 107237.
Shi, J., Wang, J., Muzenda, T.R., Qu, Y., Hou, P., Cheng, X., Liu, M., 2020. Effects of nanosilica on the hydration and hardening properties of blended cement-based materials under heat curing. J. Therm. Anal. Calorim. 141, 1317–1330.
Tang, L., He, Z., Pei, S., Han, J., Zou, M., Qin, M., Yu, Z., 2024. Hydration characteristics and pollution solidification mechanism of full solid waste electrolytic manganese residue super sulfate cement. J. Build. Eng. 84, 108563.
Tsardaka, E.-C., Stefanidou, M., 2022. Study of the action of nano-alumina particles in hydrated lime pastes. J. Build. Eng. 46, 103808.
T/CECS 737-2020, 2020. Technical Specification for Application or Road Solidified Soil. China Planning Press (in Chinese).
Wang, D., Hou, P., Stephan, D., Huang, S., Zhang, L., Yang, P., Cheng, X., 2020. SiO_2/TiO_2 composite powder deposited on cement-based materials: rhodamine B removal and the bonding mechanism. Constr. Build. Mater. 241, 118124.
Wang, X., Kim, S., Wu, Y., Liu, Y., Liu, T., Wang, Y., 2023. Study on the optimization and performance of GFC soil stabilizer based on response surface methodology in soft soil stabilization. Soils Found. 63, 101278.
Wang, R., Tang, C., Pan, X., Wang, D., Dong, Z., Zhang, X., Lu, X., 2024a. Efficient stabilization of dredged sludge with high water content using an improved bio-carbonation of reactive magnesia cement method. J. Rock Mech. Geotech. Eng. 16, 3760–3771.
Wang, J., Lu, X., Wang, J., Deng, X., Li, M., Lv, X., Zhu, C., Tan, H., 2024b. Modification of super-sulfated cement based foamed concrete with nano-ettringite. Constr. Build. Mater. 417, 135200.
Wang, S., Lang, L., Liu, Z., Pu, S., 2024c. Hardening properties, water resistance and associated micro-mechanism of nano-modified calcium sulphoaluminate cement. Case Stud. Constr. Mater. 21, e03969.
Wu, Q., Xue, Q., Yu, Z., 2021. Research status of super sulfate cement. J. Clean. Prod. 294, 126228.
Wu, Z., Zhang, H., Pu, S., Cai, G., Duan, W., Song, H., Zeng, C., Yang, Y., 2024. Synergistic preparation of geopolymer using electrolytic manganese residue, coal slag and granulated blast furnace slag. J. Build. Eng. 91, 109609.
Xing, J., Zhou, Y., Peng, Z., Wang, J., Jin, Y., Jin, M., 2023. The influence of different kinds of weak acid salts on the macro-performance, micro-structure, and hydration mechanism of the supersulfated cement. J. Build. Eng. 66, 105937.
Xu, L., Wu, K., Li, N., Zhou, X., Wang, P., 2017. Utilization of flue gas desulfurization gypsum for producing calcium sulfoaluminate cement. J. Clean. Prod. 161, 803–811.
Xu, B., Yi, Y., 2021. Soft clay stabilization using three industry byproducts. J. Mater. Civ. Eng. 33 (5), 06021002.
Xu, G., Han, Q., Geng, W., Yin, J., Liu, L., 2023. Evaluation of fiber reinforcement on the strength behaviors of dredging slurry cemented at high water content. Soils Found. 63, 101264.
Xu, F., Meng, H., Liu, W., Tang, X., Ma, W., 2024. Effect of steel slag as alkaline exciter on the properties of supersulfated cement. Mater. Lett. 369, 136631.
Yao, K., Wang, W., Li, N., Zhang, C., Wang, L., 2019. Investigation on strength and microstructure characteristics of nano-MgO admixed with cemented soft soil. Constr. Build. Mater. 206, 160–168.
Zhang, A., Yang, W., Ge, Y., Du, Y., Liu, P., 2021. Effects of nano-SiO2 and nano-Al2O3 on mechanical and durability properties of cement-based materials: a comparative study. J. Build. Eng. 34, 101936.
Zhang, W., Jin, D., Guo, X., Qin, X., Liu, X., 2023. Geoenvironmental properties of a Cr(VI)-contaminated soil treated by alkali-activated GGBS under freeze-thaw cycles: insights into Cr species transformation and microscopic mechanism. Sci. Total Environ. 903, 166450.
Zhang, W., Lang, L., Qi, Z., Wang, Y., Xue, Q., Li, J., 2025. Muti-scale analysis of solidification/stabilization (S/S) of Pb-contaminated dredged sediment using nano-SiO_2 modified cement. J. Rock Mech. Geotech. Eng. 17, 5781–5799.

Lei Lang received his PhD at Shanghai Jiao Tong University, China in 2022, and then took the positions of post-doctoral and associate professor at the Institute of Rock and Soil Mechanics, Chinese Academy of Sciences, and Yunnan University, China, respectively. His research interests include geo-environmental engineering and solid waste recycling. He is the project leader of several projects, including the National Key R&D Program of China, National Natural Science Foundation of China (NSFC), China Postdoctoral Science Foundation, and Special Research Assistant Program of the Chinese Academy of Sciences. He has published more than 20 academic SCI-indexed papers as the first or corresponding author.